FINAL REPORT

Remote-sensing-based rice mapping and crop water productivity analysis for two rice schemes in Timor-Leste

CLIENT FAO

AUTHORS Gijs Simons
Chris Hurink

DATE 31/03/2026

Remote-Sensing-Based Rice Mapping and Crop Water Productivity Analysis for two Rice Schemes in Timor-Leste

Final Report

Client

FAO

Authors

Gijs Simons
Chris Hurink

Date

30/06/2026

ADDRESS
FutureWater B.V.
Costerweg 1V
6702 AA Wageningen
The Netherlands

FutureWater

TELEPHONE **+31 317 460 050**
WEBSITE **www.futurewater.eu**

Content

Tables

Figures

1 Introduction

1.1 Context

Since gaining independence in 2002, Timor-Leste has made significant gains in peacebuilding, governance, and infrastructure with goals to achieve upper-middle income status by 2030 as laid out in its Strategy Development Plan (SDP) for 2011-2030, which places agriculture at its core. However, challenges in Timor-Leste persist, particularly with food security.

The Ministry for Agriculture, Livestock, Fisheries and Forestry (MALFF) has developed its own goal under the national SDP to “improve national food security, reduce rural poverty, support the transition from subsistence livelihoods to the commercial production of food crops, livestock, fisheries, forestry and industrial crops; and promote environmental sustainability and conservation of Timor-Leste’s natural resources.”

Under the project *TCP/TIM/390*, FAO developed a national assessment report compiling indicators for rice production and value chains and a detailed strategy for strengthening the rice industry for MALFF. To further support the goals of MALFF and strengthen the technical capacity of staff there to conduct remote-sensing-based rice mapping and crop water productivity analyses, FAO has hired FutureWater to develop a remote-sensing-based rice mapping and crop water productivity analysis for national GIS/statistics specialists at MALFF, focusing on two priority irrigation schemes (Sungai Bebui and Oebaba).

1.2 Objective

The objective of this assignment is to develop and demonstrate a remote-sensing-based rice mapping and crop water productivity methodology and analysis for national GIS/statistics specialists at MALFF. The analysis to be performed aims to meet MALFF’s immediate needs on assessing rice area and productivity. In addition, FutureWater also supports MALFF in building capacity to undertake these analyses themselves by developing a step-by-step guide on conducting a crop water productivity assessment.

2 Approach

2.1 Study area

This study focuses on two pilot rice irrigation schemes in Timor-Leste, Sungai Bebui and Oebaba, located within the municipalities of Viqueque and Covalima, respectively (Figure 1). These schemes were selected by FAO as priority areas for demonstrating the remote-sensing-based methodology to map rice extent, estimate yield, and assess crop water productivity. Both study areas represent irrigated rice landscapes where improved spatial information on rice extent, production and water productivity is needed to support agricultural planning and monitoring.

The schemes are located on the southern side of Timor-Leste, where the climate is tropical monsoonal and generally wetter than in the north of the country. Timor-Leste has a wet season that runs from December to May and a dry season from June to November, while the southern parts of the country tend to experience a longer wet season of around seven to nine months[1]. Temperatures are warm throughout the year, with only limited seasonal variation. According to local municipal sources, Viqueque experiences a rainy season extending from October / November to June and a dry season from July to September or October[2]. In Covalima, the rainy season generally runs from November to June and the dry season from July to September[3]. Viqueque is characterized as a higher-rainfall south-coast municipality with steep terrain, dense forest, and numerous rivers. Covalima combines steep hill country with wide river valleys, coastal plains with strong potential for rice production, and marshy coastal zones.

Field information collected by FAO from extension workers in Raemea–Oebaba indicates that rice is generally cultivated once a year, with land preparation taking place from December to April, planting from January to April, and harvesting from April to August. At the same time, the crop calendar is not spatially uniform, as planting dates differ between fields and communities, causing rice growth peaks to occur in different months. The Oebaba system is fully irrigated through the Kay Rala Xanana Gusmão irrigation scheme. Mixed cultivation after the rice season also appears to be limited, with farmers generally not following rice with legumes. Extension workers noted that cultivated area declined between 2019 and 2022, while crop failure occurred in 2024 due to drought and locust infestation

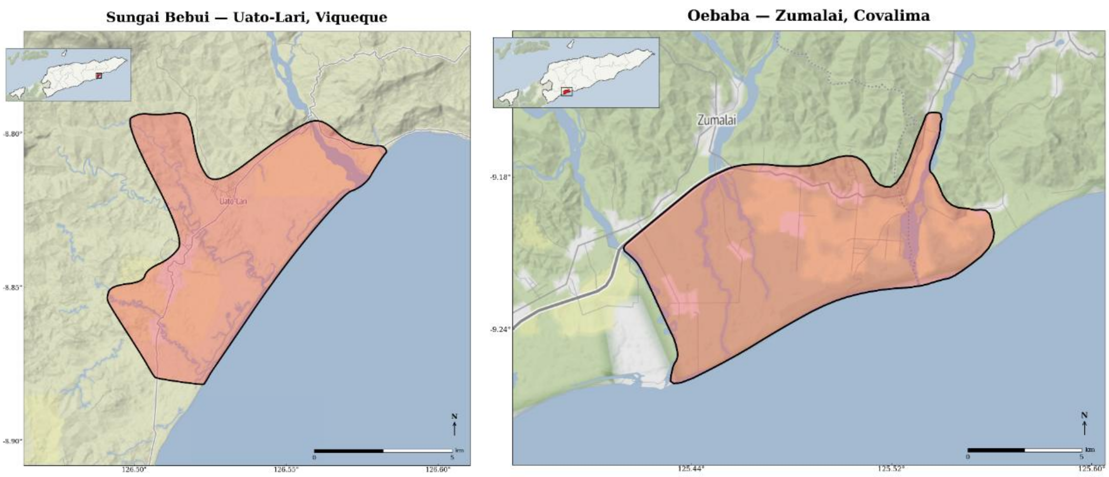

.

Figure 1: Maps of Sungai Bebui (left) and Oebaba (right) irrigation schemes

---

[1] *Climate Risk Country Profile: Timor-Leste (2021): The World Bank Group and the Asian Development Bank.*
[2] *https://viqueque.gov.tl/en/*
[3] *https://covalima.gov.tl/en/*

2.2 General approach

Figure 2 summarizes the general approach that was followed in this study. Methodological details as well as specifics regarding data sources are described in Sections 3.1 (rice and land use / land cover mapping) and 4.1 (yield and crop water productivity calculations).

Overall, the approach relies heavily on the use of satellite-derived remote sensing data, to compensate for a lack of field data on rice extents and yields in Timor-Leste. Satellite-based rice mapping and assessment of yield and water productivity is, by now, a well-established approach that has been successfully implemented around the world. Its strengths include the ability to provide spatially contiguous and quantitative assessments of crucial performance variables of agricultural systems, map remote areas, and derive temporal trends. However, applications tailored to the climatological, geographical and institutional context of Timor-Leste up to now have been scarce.

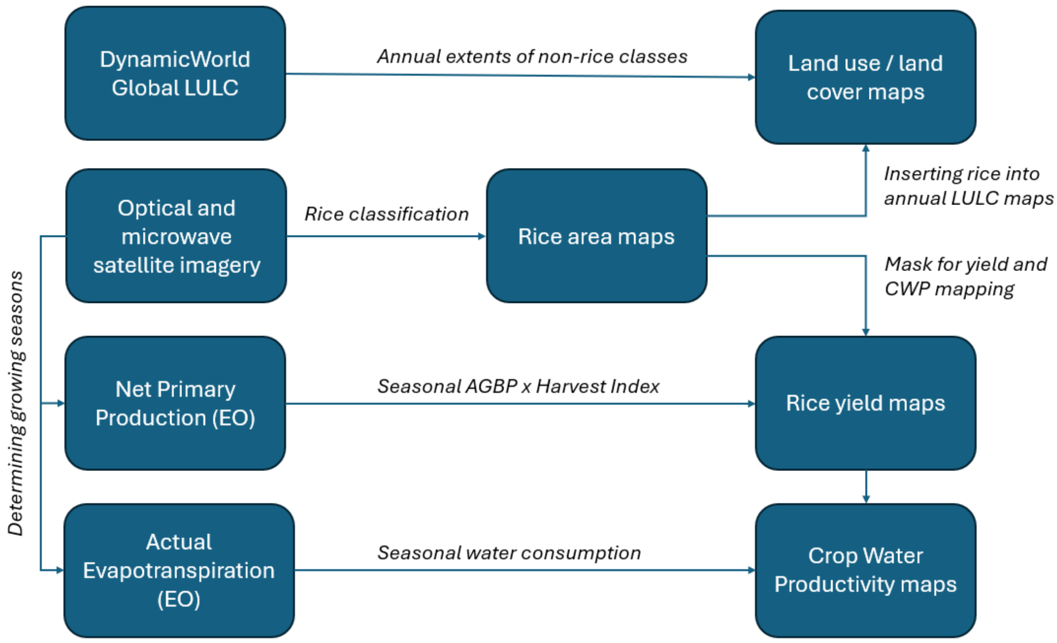

Figure 2: Flowchart of the approach, highlighting main inputs, processes and outputs of the study.

Broadly speaking, the approach brings together both primary data analysis for rice mapping based on Sentinel satellite imagery, and usage of readily available satellite-derived data products such as the FAO WaPOR v3 database and DynamicWorld land use / land cover. As shown in Figure 2, four main outputs were created from this work: annual land use / land cover maps, rice area maps, rice yield maps and crop water productivity maps. These outputs were created for each of the selected years (see Section 2.3) and irrigation systems.

All steps followed were implemented in Google Earth Engine (GEE), a cloud-based platform for geodata processing. This should facilitate future upscaling to other areas of Timor-Leste, beyond the initial two pilot irrigation schemes, as well as uptake by technical staff of MALFF.

2.3 Selection of illustrative years

To assess the impact of climate variability on rice production, three illustrative years were selected to represent “Normal,” “Wet,” and “Dry” conditions. The selection was guided by an analysis of annual rainfall data from the Viqueque and Zumalai weather stations, and verified against Sentinel-2 data availability.

2.3.1 Climate Data

As shown in Figure 1, the climatic record reveals patterns that support the selection of the following illustrative years:

- **2022 (Normal Year):** Rainfall totals across both stations are close to the multi-year average, representing stable conditions without extreme weather events. This year serves as a baseline reference for comparison with the wet and dry illustrative years.
- **2021 (Wet Year):** A distinct regional peak is observable in 2021. Both Viqueque and Zumalai recorded elevated rainfall totals compared to the baseline, indicating a widespread wet year rather than a localised anomaly.
- **2023 (Dry Year):** The available rainfall records for 2023 show reduced totals compared to both 2021 and 2022. This declining trend is consistent with the onset of drier conditions associated with the 2023–2024 El Niño event.

It should be noted that the station records for 2022 and 2023 contain data gaps, with only 8–9 months of valid observations available. However, the months with data show patterns consistent with the classifications above.

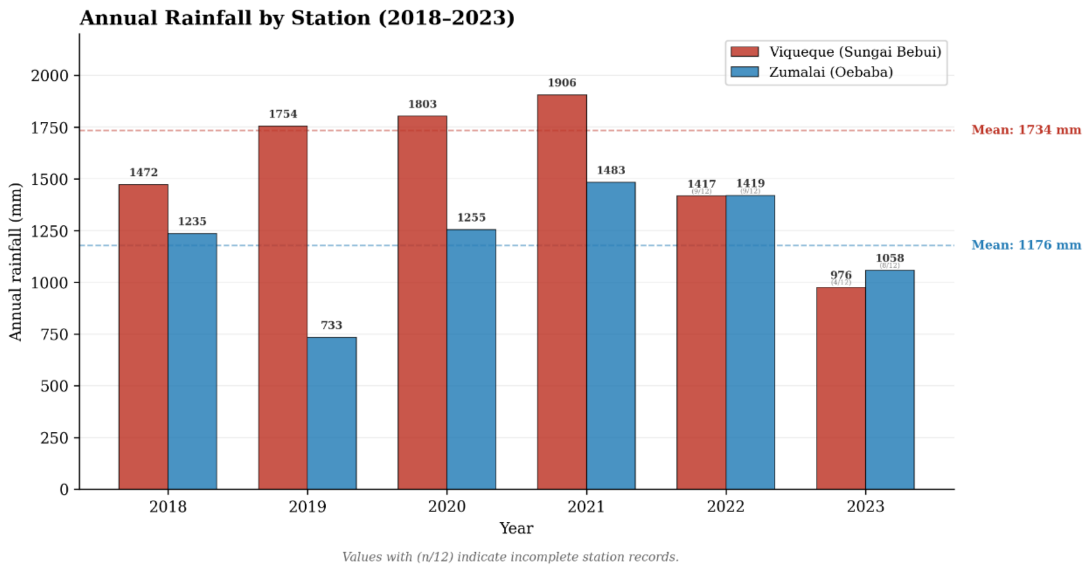

Figure 1: Annual rainfall recorded at the Viqueque and Zumalai weather stations (2018–2023). Incomplete station records are indicated with the number of months with valid observations.

2.3.2 Sentinel-2 Data Availability

The analysis period starts from 2019 due to limitations in the Sentinel-2 cloud masking approach. From 2019 onwards, the Copernicus Sentinel-2 Level-2A product provides a pixel-based Scene Classification Layer (SCL), which enables accurate identification and masking of clouds, cloud shadows, and cirrus at the individual pixel level. This is critical for the NDVI-based rice detection algorithm described in Section 3.1, as undetected cloud contamination can produce false vegetation peaks that mimic rice growth signatures.

Prior to 2019, Level-2A products with the SCL band were not consistently available for Timor-Leste. For these earlier years, cloud filtering relies on granule-level metadata (CLOUDY_PIXEL_PERCENTAGE), which provides only a single cloud cover estimate for the entire image tile rather than a per-pixel classification. This coarser approach is less reliable in tropical monsoon climates where partial cloud cover is common.

Figure 2 shows the number of clear observation days per year for both study areas. From 2019 onwards, both areas consistently have 29–45 cloud-free observation days per year, providing sufficient temporal coverage for monthly NDVI compositing and peak detection. All three illustrative years have adequate data density for reliable analysis, confirming that the year selection was primarily guided by the climatic conditions rather than constrained by data availability.

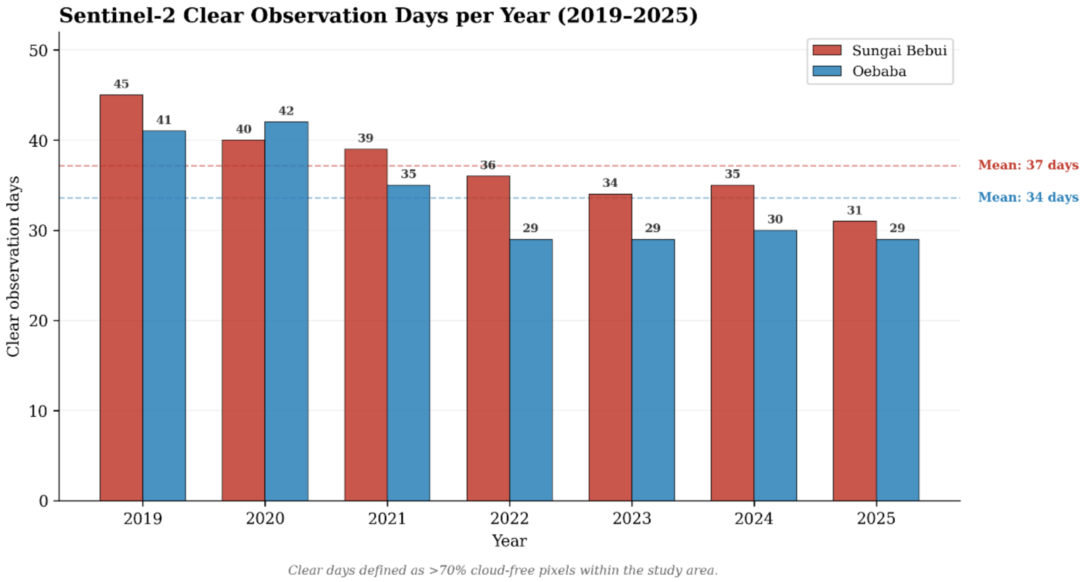

Figure 2: Number of cloud-free Sentinel-2 observation days per year for both study areas (2019–2025), based on pixel-level SCL cloud masking with a minimum 70% clear-sky threshold.

3 Land Use / Land Cover and Rice Area Mapping

3.1 Methodology

The rice area mapping methodology combines optical and radar satellite data with machine learning classification within the Google Earth Engine (GEE) cloud computing environment. The approach builds upon and extends the work of Ginting et al. (2025)[1], who developed a high-resolution rice cropping intensity product for Southeast Asia using Sentinel-1 and Sentinel-2 time series. The methodology was applied independently for each year in the 2019–2025 period, producing annual rice extent maps at 10m spatial resolution for the Sungai Bebui and Oebaba study areas.

All data sources used are publicly available and freely accessible, and all processing scripts are implemented in the GEE JavaScript API to facilitate replication by MALFF GIS / statistics specialists.

3.1.1 Input data

Three satellite-derived data sources were used:

- **Sentinel-2 optical imagery:** Level-2A surface reflectance imagery (Copernicus S2_SR_HARMONIZED collection) was acquired for the study region over an extended 16-month window spanning from November of the preceding year through February of the following year. Cloud and cloud shadow contamination was addressed using the Scene Classification Layer (SCL), whereby pixels classified as cloud shadow, medium- or high-probability cloud, or thin cirrus were masked. Scenes with less than 20% clear-sky coverage over the region of interest were discarded. From the retained imagery, the Normalized Difference Vegetation Index (NDVI) was computed per pixel as:

$$NDVI = \frac{\rho_{NIR} - \rho_{Red}}{\rho_{NIR} + \rho_{Red}}$$

  where ρ_{NIR} and ρ_{Red} denote the surface reflectance in the near-infrared (Sentinel-2 Band 8, 842 nm) and red (Band 4, 665 nm) spectral bands, respectively. Monthly median composites were generated for each calendar month, yielding a spatially continuous 12-band NDVI time series per analysis year.

- **Sentinel-1 C-band SAR backscatter.** Ground Range Detected (GRD) imagery acquired in Interferometric Wide (IW) swath mode was used to derive monthly median composites of VH-polarised backscatter (in dB). The same 16-month temporal window and monthly compositing approach were applied. The VH polarisation channel is particularly suited for rice mapping, as flooded paddy fields produce a distinctive low-backscatter signal caused by specular reflection of smooth water surfaces under C-band radar.

- **Dynamic World land cover.** The Google Dynamic World near-real-time land use / land cover (LULC) product was used to generate an initial cropland mask for each analysis year. Pixels classified as cropland or flooded vegetation in any observation during the year were retained as candidate rice-growing areas. This mask constrained all subsequent analysis to agriculturally plausible locations, excluding built-up areas, permanent water bodies, forest, and bare ground.

[1] *Ginting, F. I., Rudiyanto, R., Fatchurrachman, Mohd Shah, R., Che Soh, N., Eng Giap, S. G., Fiantis, D., Setiawan, B. I., Schiller, S., Davitt, A., and Minasny, B.: High-resolution maps of rice cropping intensity across Southeast Asia, Scientific Data, 12, 1408, 10.1038/s41597-025-05722-1, 2025.*

3.1.2 Temporal compositing framework

To capture the full phenological cycle of rice — including pre-season field preparation and flooding, the vegetative growth phase, and post-harvest senescence — a 16-month compositing window was adopted for peak detection purposes. This window extends from November of the preceding year through February of the following year, centered on the January–December analysis year. The flanking months (November–December prior, January–February following) serve as lookback and forward-look context for the detection of pre-peak flooding signals and post-peak harvest drops, respectively. Only the 12 months within the analysis year itself were considered as candidate peak months.

3.1.3 Rule-based rice phenology detection

A per-pixel phenological screening algorithm was developed to identify rice growth signatures by jointly evaluating four spectral-temporal conditions. For each of the 12 candidate months within the analysis year, the algorithm assessed whether the pixel exhibited characteristics consistent with a paddy rice cropping cycle:

1. **Peak greenness.** The NDVI of the candidate month was required to exceed 0.5, corresponding to the dense green canopy cover of mature rice.
2. **Pre-peak flooding or bare soil.** The minimum NDVI in the one to two months preceding the candidate peak was required to fall below 0.4, consistent with the low vegetation cover associated with transplanting into flooded or bare fields.
3. **SAR flooding signature.** The minimum VH backscatter in the one to three months preceding the candidate peak was required to fall below −18 dB, consistent with the presence of standing water on paddy fields.
4. **Post-peak harvest drop.** A decline in NDVI of at least 0.05 was required in the one to two months following the candidate peak, reflecting canopy senescence and harvest.

For each pixel, the candidate month with the highest NDVI satisfying all four conditions was selected as the primary rice peak. The prominence of the detected peak — defined as the difference between peak NDVI and the pre-peak minimum — was required to exceed 0.10 to exclude low-amplitude fluctuations not indicative of rice cultivation. Two further whole-year filters were applied: the coefficient of variation (CV) of the annual NDVI series was required to exceed 0.15, ensuring sufficient temporal variability consistent with seasonal cropping; and the annual median NDVI was required to remain below 0.7, excluding areas with dense perennial vegetation such as forest. The annual maximum VH backscatter was required to exceed −17 dB, filtering out terrain and permanent water bodies where VH backscatter remains consistently low.

3.1.4 Peak month detection

The detected peak month identifies the timing of maximum rice canopy development for each pixel and is used downstream to define the per-pixel growing season window for yield and water productivity estimation (Section 4).

Field confirmation from FAO extension workers (March 2026) established that rice in both study areas is cultivated once per year. The crop calendar varies spatially within each scheme, with planting occurring over a range of months depending on local conditions and water availability. Consequently, the analysis focuses on the peak NDVI month as the primary temporal descriptor of rice phenology, rather than assigning discrete growing seasons.

3.1.5 Machine learning classification and post-processing

While the rule-based approach provides high-confidence rice detections, its strict thresholds inevitably omit some genuine rice pixels that fail one or more conditions — for instance, due to persistent cloud cover during the peak month, atypical planting timing, or weak SAR flooding responses. To recover these pixels and improve spatial completeness, a Random Forest supervised classifier was trained and applied within the cropland mask. This procedure followed three steps:

1. **Training data generation.** The rule-based rice mask was morphologically eroded (30 m circular kernel) to extract spatially interior, high-confidence rice pixels as positive training samples. Cropland pixels outside the rule-based rice mask were similarly eroded to generate negative (non-rice) training samples. Approximately 8,000 samples per class were drawn at 30 m spacing across the study area.
2. **Training.** The classifier was trained on a feature stack comprising 28 bands: the 12 monthly NDVI composites, the 12 monthly VH backscatter composites, and four phenological summary variables derived from the peak detection step (peak calendar month, peak NDVI, prominence, and peak detection score).
3. **Classification.** A Random Forest ensemble of 50 decision trees was applied to all pixels within the cropland mask. The resulting classification extends the rice extent to areas that share the spectral-temporal profile of confirmed rice fields but did not strictly satisfy all rule-based thresholds.

Subsequently, spatial noise was removed while preserving field boundaries. This procedure included application of a focal mode filter with a 5 m circular kernel to eliminate isolated misclassified pixels. Also, **c**onnected components (eight-connectivity) smaller than 25 pixels (approximately 0.25 ha) were removed, corresponding to areas below the minimum plausible paddy field size in the study region. Finally, gaps within the rice mask smaller than 25 pixels were filled to close small internal voids caused by individual pixel-level misclassifications within otherwise contiguous paddy areas.

3.1.6 Peak month assignment for classifier-rescued pixels

Pixels classified as rice by the Random Forest but not detected by the rule-based phenology algorithm lack an explicit peak month. For these pixels, the peak month was assigned using a focal mode filter (50 m radius) that propagates the most common peak month from neighbouring rice pixels. This ensures all rice pixels have a valid peak month for downstream growing season definition and yield estimation.

3.1.7 Multi-year aggregation

The annual classification results were combined across the full 2019–2025 period to produce aggregate spatial products:

1. **Rice frequency.** The number of years (1–7) in which each pixel was classified as rice, providing a measure of the persistence and stability of rice cultivation at each location.
2. **Confident rice mask.** A binary layer retaining only pixels classified as rice in at least four of the seven years, providing a spatially conservative estimate of persistent rice-growing areas.

3.1.8 Output products

For each analysis year, the pipeline exports three combined multi-year products as GEE assets: (i) a classification image containing rice extent and peak calendar month per year; (ii) a 12-band monthly NDVI composite per year; and (iii) a 12-band monthly VH backscatter composite per year. An additional KMZ file containing vectorised rice polygons for all years is exported to Google Drive for use in external GIS applications. The combined multi-year asset structure enables instant loading in the visualisation script without requiring re-computation.

3.1.9 Land Use / Land Cover Mapping

To place the rice classification results within the broader geographical context and to visualise the distribution of rice versus other crops, the annual rice extent maps were integrated into the Dynamic World (DW) land use / land cover product. For each analysis year the DW annual mode land cover map, representing the most frequently assigned class per pixel, was used as a baseline. This baseline was then modified in two steps:

1. **Rice overlay.** Pixels classified as rice by the mapping pipeline (Section 3.1) were assigned a new "Rice" class, overriding whatever land cover class DW had assigned. This ensures that the rice extent derived from the dedicated phenological and machine learning approach takes precedence over the generic DW cropland class.
2. **Other crops distinction.** Pixels to which DW assigned the cropland class (class 4) in at least one observation during the analysis year, but which were not identified as rice, were reclassified as "Other crops." This separates non-rice agricultural activity from the broader DW cropland category.

All remaining DW classes were retained. The resulting custom land cover map thus contains the full DW class set supplemented with two additional agricultural categories: rice and other crops.

3.2 Results

3.2.1 Rice area maps

The rice classification algorithm was run for Sungai Bebui and Oebaba schemes for the full 2019 – 2025 period, for which the results are plotted in Figure 3. Spatially, Figure 4 presents the results of the rice area mapping, for the three selected years. Both the maps and the graph show that there is considerable interannual variability of the total extent of cropped rice area in both schemes. There is, however, not a consistent, direct relation with precipitation amounts for the selected years, which represent normal (2022), wet (2021) and dry (2023) conditions. This suggests that other potential causes, such as reliability of water delivery by the irrigation canals, access to labor or seeds, pests, or other factors, play a more decisive role. Figure 5 synthesizes the annual results in 2019 – 2025 rice frequency maps.

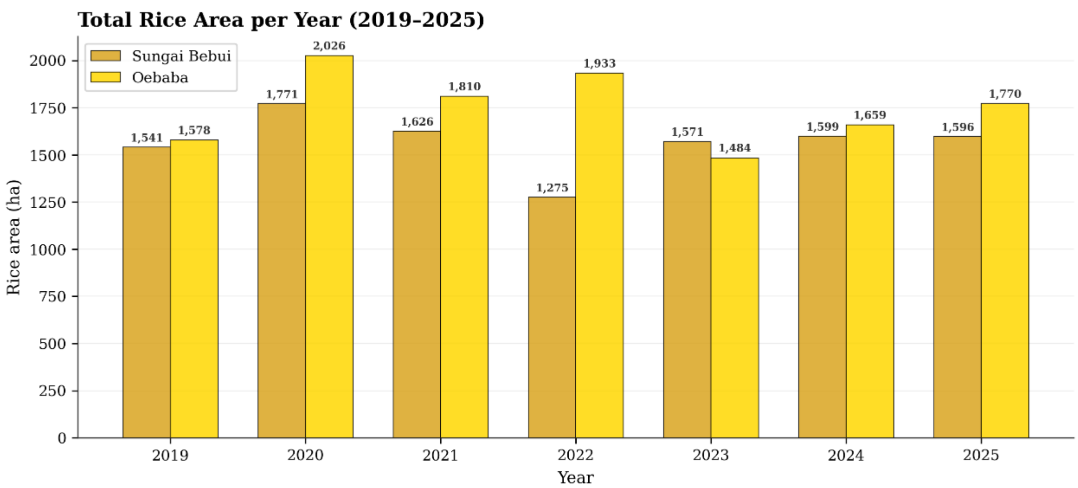

Figure 3: Rice areas for Sungai Bebui (left) and Oebaba (right) irrigation schemes in 2019 – 2025.

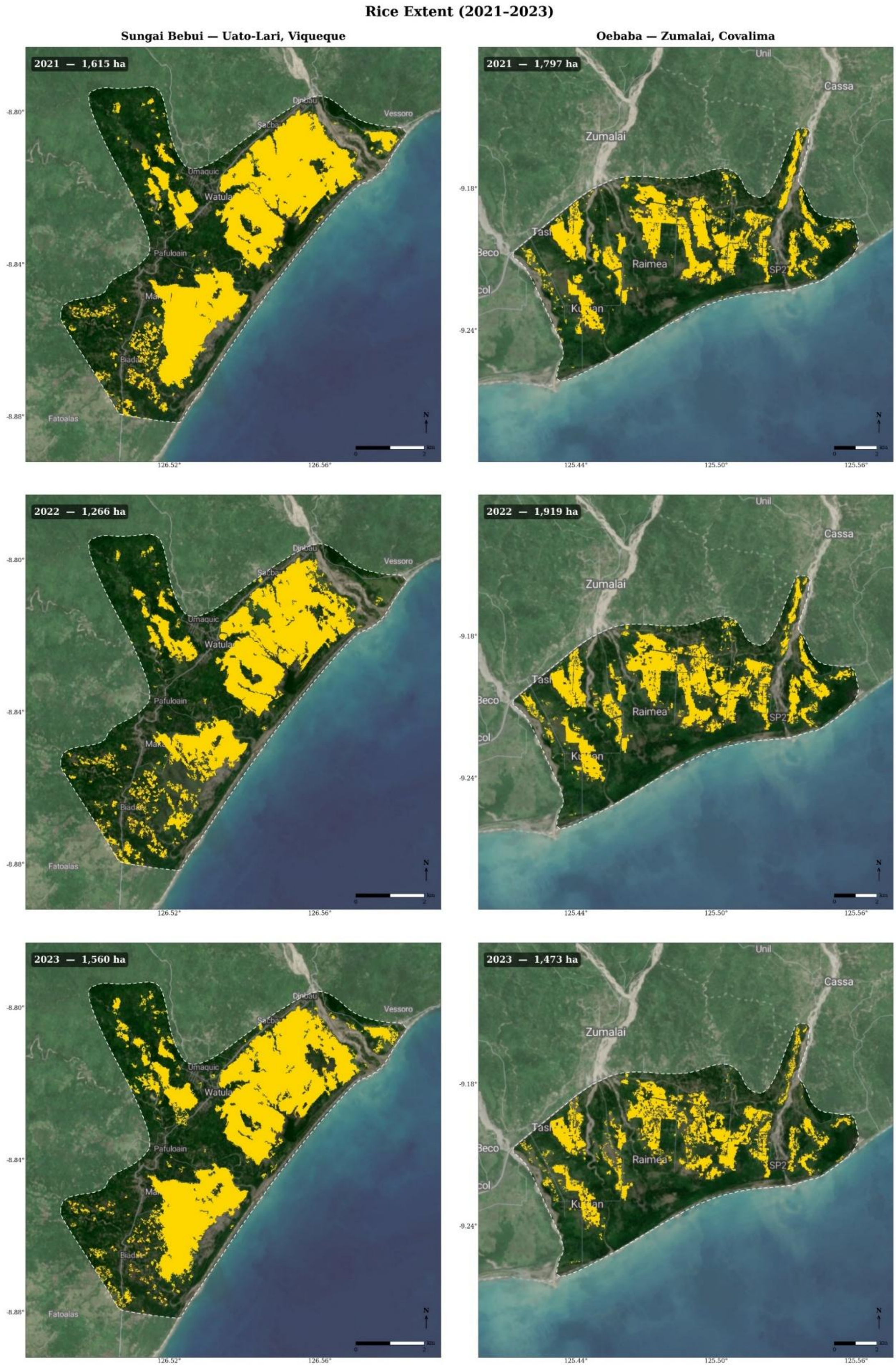

Figure 4: Rice area maps for Sungai Bebui (left) and Oebaba (right) irrigation schemes in 2021, 2022 and 2023. Total area classified as rice is indicated in the maps

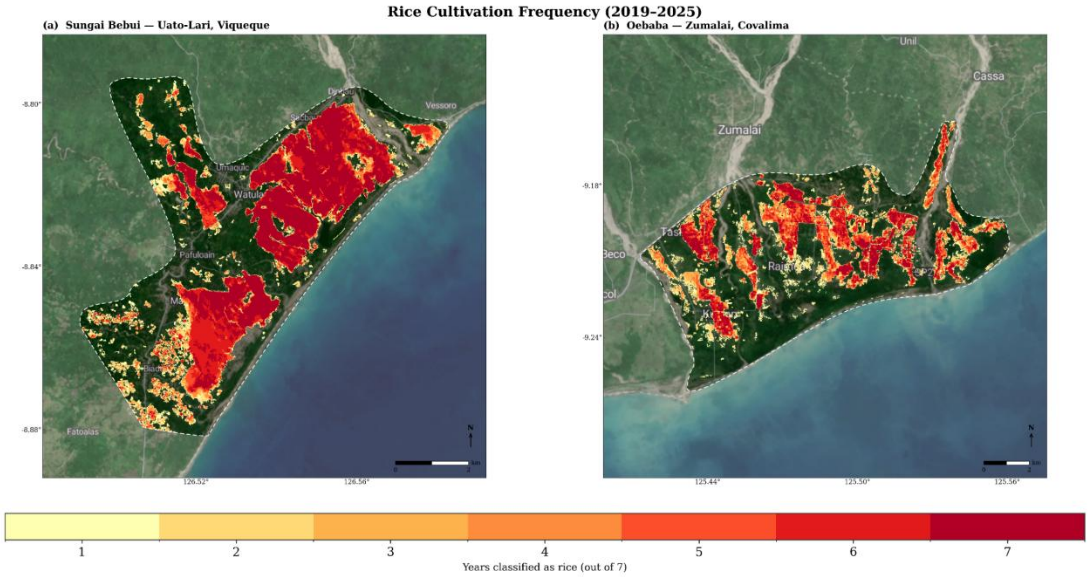

Figure 5: Frequency of rice cultivation (number of years a pixel is classified as rice) in Sungai Bebui (left) and Oebaba (right) irrigation schemes, 2019 – 2025

To highlight differences in farmer choices and cropping seasons, Figure 6 maps the peak NDVI (greenness) month across each of the irrigation schemes. Figure 7 compares the two schemes in terms of the peak NDVI month, clearly showcasing substantial differences between the two areas. By far the largest part of the area classified as rice in Sungai Bebui sees its peak greenness month in July or June, whereas the peaks in Oebaba typically lie earlier in the year (May or April).

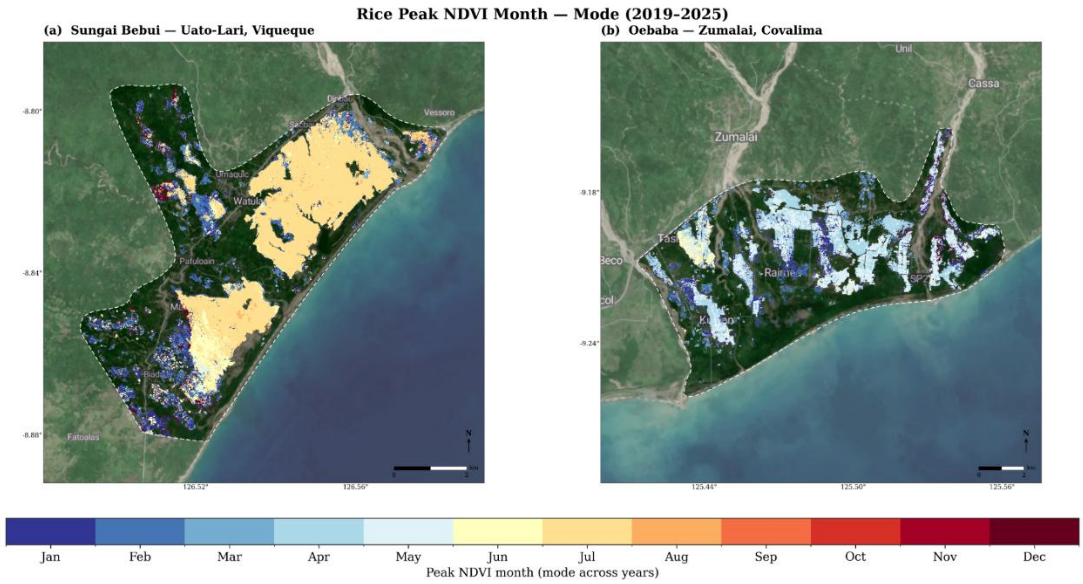

Figure 6: Maps of peak NDVI months for rice areas in Sungai Bebui (left) and Oebaba (right) schemes

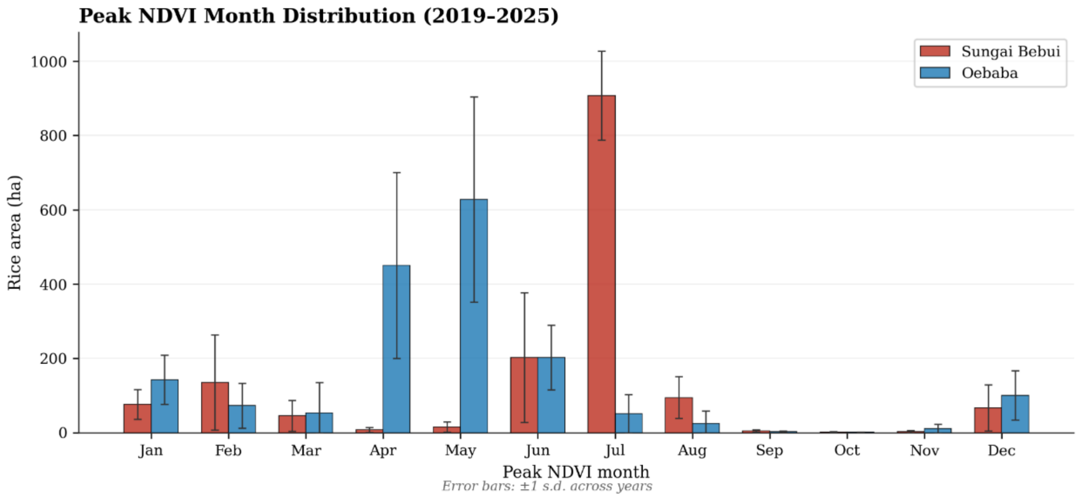

Figure 7: Comparison of peak NDVI months for rice areas in Sungai Bebui (left) and Oebaba (right) schemes

To validate the results of the remote sensing assessment regarding the rice season timings, satellite-derived peak NDVI months were compared with the latest cropping calendars for Sungai Bebui and Oebaba obtained by FAO (Figure 8). The results support the findings of the satellite-based approach, as the peak NDVI months are typically identified late in the growing cycle of the rice crop according to the crop calendar. For Oebaba, it is striking that the diversity of farmer choices in terms of the cropping season is much higher than in Sungai Bebui, which is also reflected in the satellite-based assessment, as the peak NDVI value is less concentrated in a single month but spread over May, April and June, among others. Fields with peak months in December, January or February may point at the occurrence of mixed cropping, or a second rice season. This, however, requires field data collection for validation.

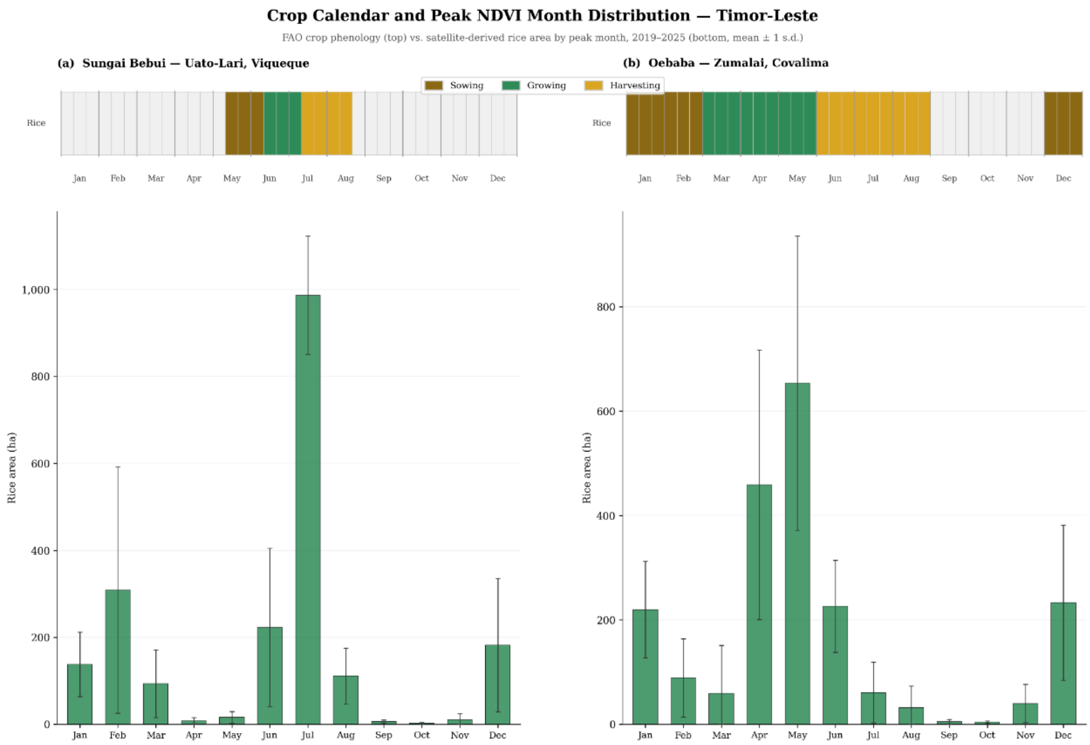

Figure 8: Comparison between crop calendar for rice in Sungai Bebui (a) and Oebaba (b), based on field surveys, and the peak NDVI month determined from satellite imagery

Table 1 presents an overview of annual rice extents in Sungai Bebui and Oebaba for 2019 – 2025, along with the predominant peak NDVI month.

Table 1: Overview of rice areas in the two pilot irrigation schemes in 2019 – 2025, and the predominant peak greenness month in each year

Year	Sungai Bebui		Oebaba	
	Area (ha)	*Peak month*	*Area (ha)*	*Peak month*
2019	1.540	Jul	1.577	May
2020	1.770	Jul	2.026	May
2021	1.626	Jul	1.809	Apr
2022	1.274	Jul	1.932	May
2023	1.570	Jul	1.483	May
2024	1.598	Jul	1.658	Apr
2025	1.596	Jul	1.770	Apr
Average	**1,568**		**1,751**	

3.2.2 Land use / land cover maps

Annual land use / land cover maps for Sungai Bebui and Oebaba are shown in Figure 9. This integrated land use / land cover product enables a yearly comparison of the spatial distribution of rice relative to other forms of cropland, providing insight into inter-annual variability in crop choice at the field level. When examining the full 2019–2025 analysis period, these maps reveal which fields are consistently dedicated to rice, which alternate between rice and other crops, and which areas of the agricultural landscape are used exclusively for non-rice cultivation.

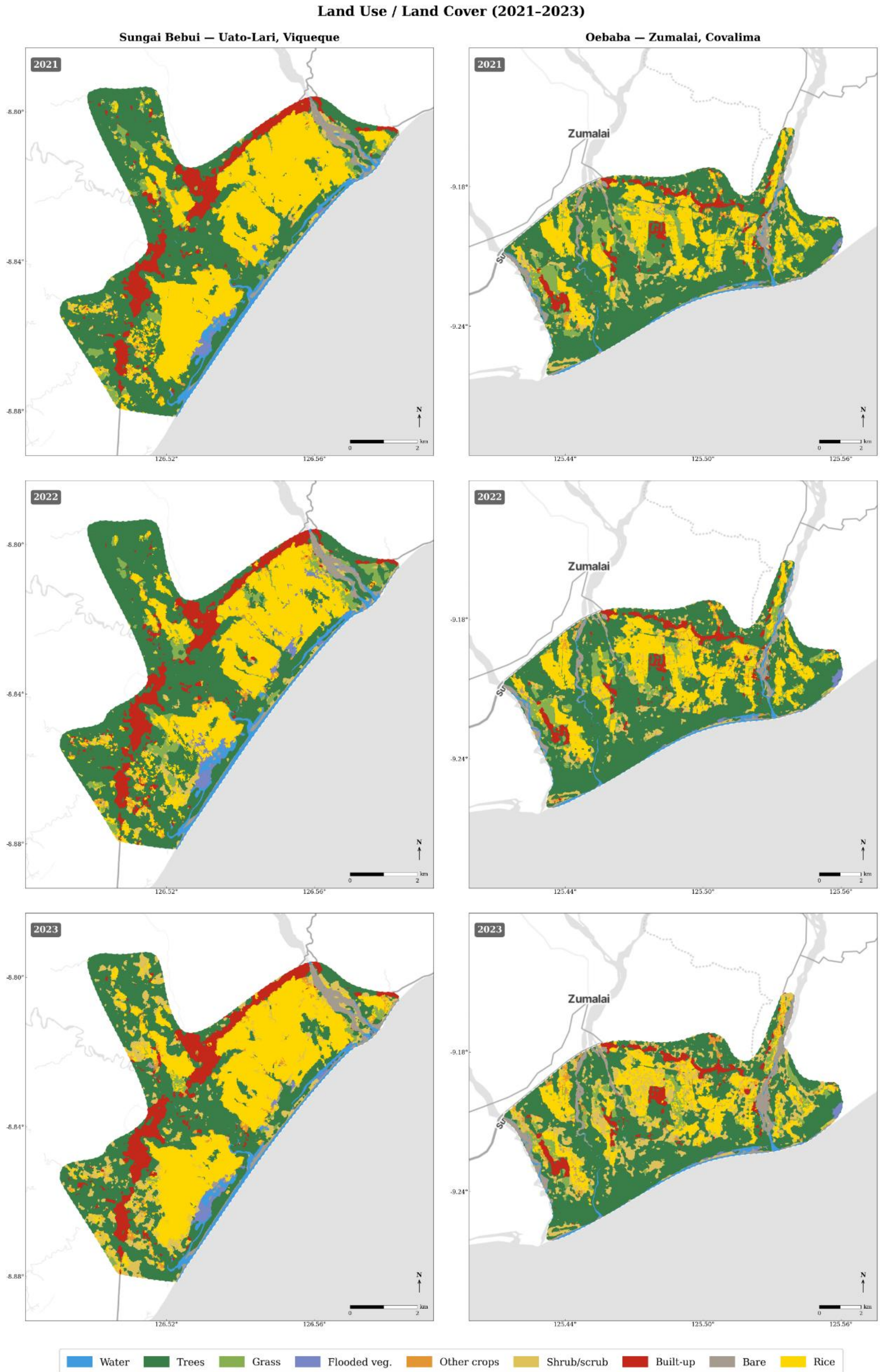

Figure 9: Yearly land use/land cover maps for Sungai Bebui (left) and Oebaba (right) in 2021, 2022 and 2023

4 Rice Yield and Water Productivity Assessment

To complement the rice extent mapping presented in Section 3, rice yield and crop water productivity (CWP) were estimated for three illustrative years (2021, 2022, and 2023) using globally available remote sensing products. The analysis combines the rice classification results with evapotranspiration and biomass productivity data from the FAO WaPOR v3 database[1].

4.1 Methodology

4.1.1 Data sources

Rice yield and CWP were derived from two dekadal (10-day) datasets provided by the FAO WaPOR v3 database, accessed through Google Earth Engine:

- **Actual Evapotranspiration and Interception (AETI).** Dekadal mean daily rates (mm/day) at approximately 250 m spatial resolution, representing the total water consumed by vegetation through transpiration and soil evaporation.
- **Net Primary Production (NPP).** Dekadal mean daily rates (g C/m²/day) at approximately 250 m spatial resolution, representing the net carbon fixed by vegetation through photosynthesis.

Both datasets were converted from mean daily rates to dekadal totals by multiplying each image by the number of days in the corresponding dekad (10 days for dekads 1 and 2; remaining days in the month for dekad 3). Monthly totals were then computed by summing the dekadal values within each calendar month.

4.1.2 Growing season definition

The growing season was defined on a per-pixel basis using the peak NDVI month identified in the rice classification (Section 3). For each rice pixel, the growing season spans from three months before to one month after the peak NDVI month, resulting in a five-month window that captures the full crop cycle from planting through harvest. This approach accounts for spatial variability in planting and harvesting dates within each irrigation scheme. For pixels with wrap-around seasons (e.g., November to March), the aggregation handles the year boundary accordingly.

In this way, the methodology applied for this study goes well beyond the typical approach followed for estimating crop yields and CWP, which relies on literature-based cropping calendars assumed spatially homogeneous for a particular area.

4.1.3 Spatial downscaling

The native resolution of WaPOR v3 (~250 m) is substantially coarser than the Sentinel-2-based rice classification (10 m). To produce yield and CWP maps at the rice pixel level, a two-step spatial downscaling approach was applied:

1. **Bilinear resampling**. Each dekadal WaPOR image was resampled from its native resolution (~250 m) to the 10 m Sentinel-2 grid using bilinear interpolation. This resampling is applied prior to temporal aggregation to ensure that the per-pixel growing season, which is defined individually for each 10 m rice pixel based on its peak NDVI month, can be computed at the classification scale. Without this step, the coarseness of the WaPOR scale would impose uniform values across ~625 Sentinel-2 pixels per WaPOR cell, resulting in blocky artefacts in

[1] *FAO. (2023). WaPOR v3: Water Productivity through Open access of Remotely sensed derived data, Version 3.0 [Dataset]. Food and Agriculture Organization of the United Nations.* https://data.apps.fao.org/catalog/dataset/wapor-v-3

the seasonal totals. Bilinear interpolation produces smooth spatial gradients that better reflect the continuous nature of evapotranspiration and productivity fields.

2. **NDVI-weighted refinement**. Within each local neighbourhood (~125 m radius coinciding with the native WaPOR pixel size), NPP and AETI values were further adjusted based on the ratio of each pixel's seasonal mean NDVI to the local neighbourhood mean NDVI. Pixels with above-average vegetation vigour receive proportionally higher NPP and AETI values, while less vigorous pixels receive lower values. The weighting factor was clamped to the range 0.5–2.0 to prevent extreme outliers. This approach preserves the overall NPP and AETI budgets at the WaPOR scale while adding within-field spatial variability informed by the high-resolution Sentinel-2 NDVI data.

4.1.4 Yield estimation

Seasonal NPP (g C/m²) was converted to above-ground biomass production (AGBP) and subsequently to rice yield using the following chain of conversions (FAO, 2020):

$$AGBP\ (kg\ DM/ha)\ =\ NPP\ (g\ C/m^2)\ \times\ (1\ /\ fc)\ \times\ (1\ -\ fr)\ \times\ 10$$

where *fc* = 0.45 is the carbon fraction of dry matter, i.e., carbon constitutes approximately 45% of plant dry matter (IPCC, 2006)[1]; *fr* = 0.25 is the below-ground (root) fraction of total biomass, such that 75% of total biomass is above-ground; and the factor 10 converts from g/m² to kg/ha.

Rice grain yield was then estimated as:

$$Yield\ (kg/ha)\ =\ AGBP\ \times\ HI$$

where *HI* is the harvest index, defined as the ratio of grain yield to total above-ground biomass.

Evidence of HI values for Timor-Leste is extremely scarce. National-level average rice yields are reported between 2 - 3 t/ha (FAOSTAT), with a value of 3.6 t/ha reported for Maliana, a well-managed irrigated scheme[2]. Noting that typical rice aboveground biomass in tropical lowland systems is around 8 – 12 t/ha, a fixed *HI* of 0.40 was applied uniformly across all years and pixels. Determining a spatially variable or stress-corrected harvest index was not feasible due to the absence of field calibration data for the study areas.

4.1.5 Crop water productivity

Crop water productivity expresses the amount of grain produced per unit of water consumed:

$$CWP\ (kg/m^3) = Yield\ (kg/ha)\ /\ Seasonal\ AETI\ (m^3/ha)$$

where 1 mm of evapotranspiration equals 10 m³/ha. CWP provides a measure of how efficiently water is converted into harvestable crop output and allows comparison across years and between the two irrigation schemes.

4.2 Rice Yield Assessment

For all area cropped by rice in Sungai Bebui and Oebaba in 2021 – 2023, Figure 10 maps the yield in tonnes per hectare. Maps of seasonal Above-Ground Biomass Production (AGBP) used in the yield calculation are included in the Annex to this report. The maps allow for distinguishing sections of the irrigation schemes based on a higher or lower land productivity.

---

[1] *IPCC. (2006). 2006 IPCC Guidelines for National Greenhouse Gas Inventories. Volume 4: Agriculture, Forestry and Other Land Use (S. Eggleston, L. Buendia, K. Miwa, T. Ngara, & K. Tanabe, Eds.). Institute for Global Environmental Strategies (IGES). https://www.ipcc.ch/report/2006-ipcc-guidelines-for-national-greenhouse-gas-inventories/*

[2] *Fernandes, P.J.; Nagai, M. Mapping Rice Cropping Systems in Data-Scarce Regions Using NDVI Time-Series and Dynamic Time Warping Clustering: A Case Study of Maliana, Timor-Leste. Appl. Sci.* ***2025****, 15, 12544. https://doi.org/10.3390/app152312544*

Figure 10: Rice yield maps for Sungai Bebui (left) and Oebaba (right) irrigation schemes in 2021, 2022 and 2023. Average rice yield is indicated in the maps

Figure 11 and Table 2 present key information on the average rice yield in each scheme per year, as well as an indication of the spatial variability by means of the 10^{th} and 90^{th} percentile values. Rice production fluctuates typically around 3 t/ha on average. However, it is important to note the significant variability occurring within the schemes, which becomes apparent by comparing P10 and P90 values. This suggest that even within the boundary conditions of a single irrigation scheme, differing circumstances lead to considerable differences in land productivity. The nature of these factors (farmer decisions, reliability of local water supply, seed quality, or others) would need to be further investigated in the field. Such follow up research can be guided by the results of the satellite-based analysis, which allows for pinpointing the fields where relatively high and low yields were obtained. Furthermore, the figures demonstrate how remote sensing-based assessments can be used for intercomparing different irrigation schemes. For the two pilot schemes, differences in average rice yields are relatively limited, and not consistent over the three years.

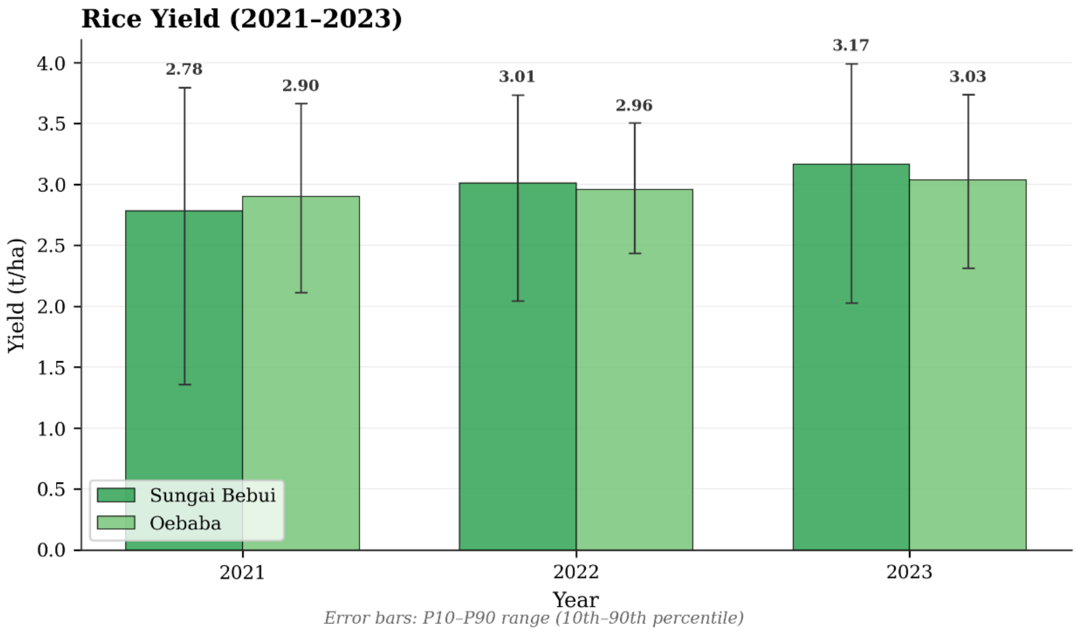

Figure 11: Rice yields for Sungai Bebui and Oebaba schemes in 2021, 2022 and 2023.

Table 2: Average, P10 and P90 rice yields for Sungai Bebui and Oebaba schemes in 2021, 2022 and 2023

Year	Sungai Bebui		Oebaba	
	Mean (t/ha)	[P10–P90]	Mean (t/ha)	[P10–P90]
2021	2.78	[1.36–3.79]	2.90	[2.11–3.66]
2022	3.01	[2.04–3.73]	2.96	[2.44–3.50]
2023	3.17	[2.03–3.99]	3.03	[2.31–3.74]

Rice yields found for Sungai Bebui and Oebaba at the higher end of the reported amounts in FAOSTAT for the last 10 years at the national level, which is realistic as the national-scale values combine rainfed and irrigated rice. Calculated yields for the pilot schemes are somewhat lower than the 3.6 t/ha reported for the Maliana irrigation scheme[1]. These figures cannot be seen, however, as fully independent resources for comparison, as they were used to inform the fixed Harvest Index value assumed in this study. More independent field data collection is required to verify the calculated yields, with *HI* and *fr* being typical calibration parameters.

[1] *Fernandes, P.J.; Nagai, M. Mapping Rice Cropping Systems in Data-Scarce Regions Using NDVI Time-Series and Dynamic Time Warping Clustering: A Case Study of Maliana, Timor-Leste. Appl. Sci.* ***2025****, 15, 12544.* *https://doi.org/10.3390/app152312544*

4.3 Crop Water Productivity Assessment

Based on the rice yields and the seasonally aggregated AETI obtained from the FAO WaPOR database, Figure 12 presents the CWP maps for rice in the Sungai Bebui and Oebaba schemes in the three selected years. The underlying seasonal AETI maps are included in the Annex to this report.

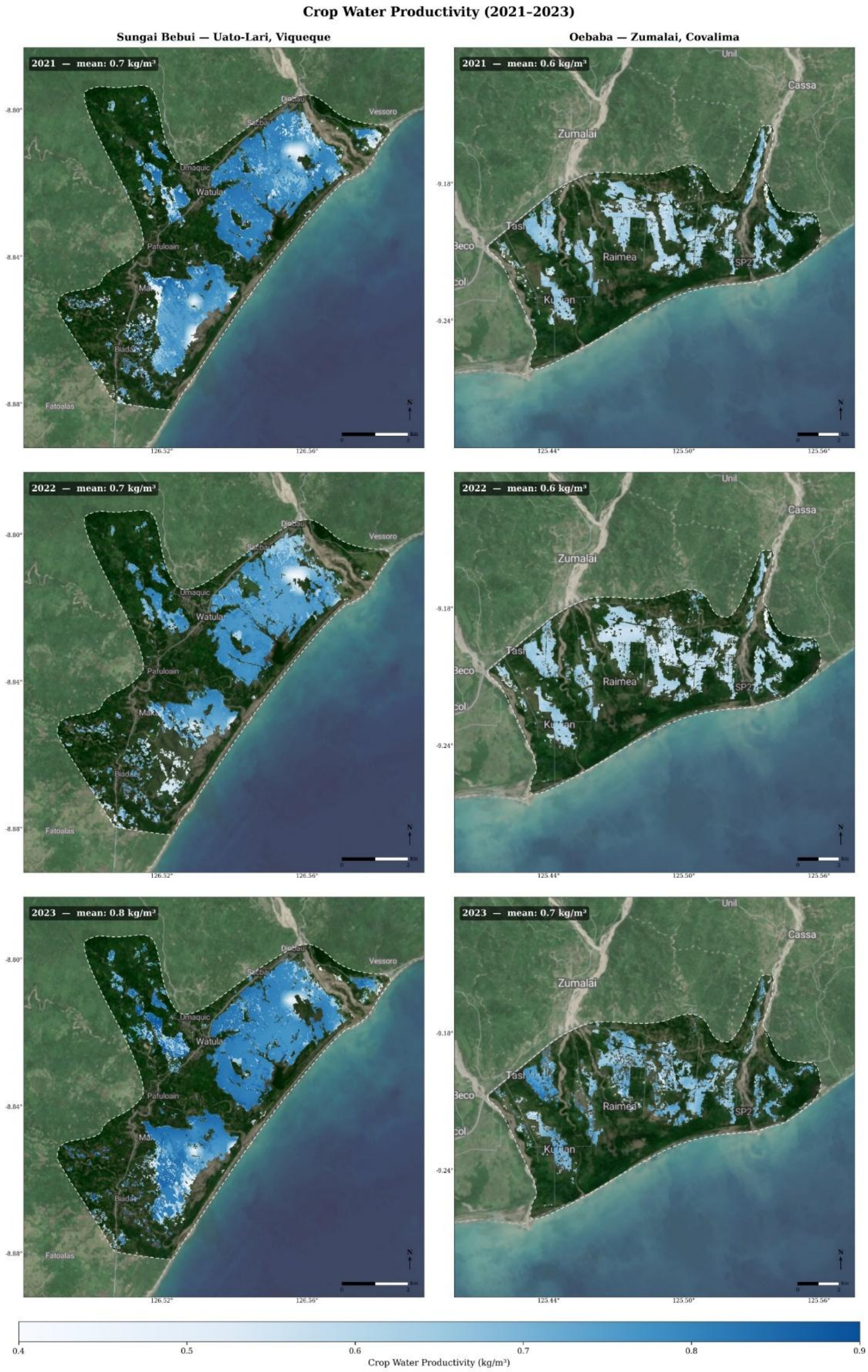

Figure 12: Rice water productivity maps for Sungai Bebui (left) and Oebaba (right) schemes in 2021, 2022 and 2023. Average CWP is indicated in the maps

These CWP maps help reveal whether water is being converted efficiently into biomass or yield. This makes CWP more informative than looking at yield or evapotranspiration alone. A field can have high production but also very high water consumption, or low water use but poor production. As the CWP assessment is spatially explicit, the maps help identify underperforming areas, hotspots of water stress, and locations where improvements in irrigation or agronomic management may have the highest benefit. In Figure 12, darker blue fields are particularly well performing (CWP “champion farmers”), whereas white areas are at the lower end of the CWP range.

Figure 13 and Table 3 present the mean rice water productivity in the two irrigation schemes during 2021 – 2023, as well as the P10 and P90 values as a measure of variability. Overall, CWP in Oebaba is consistently somewhat lower than CWP in Sungai Bebui. When comparing CWF findings with the yield discussed in Section 4.2, the added value of evaluating CWP becomes apparent; although in 2022 and 2023 Sungai Bebui achieved a higher average yield than Oebaba, it consumed less water to achieve this rice production, illustrating an overall more efficient use of water resources at the scheme level.

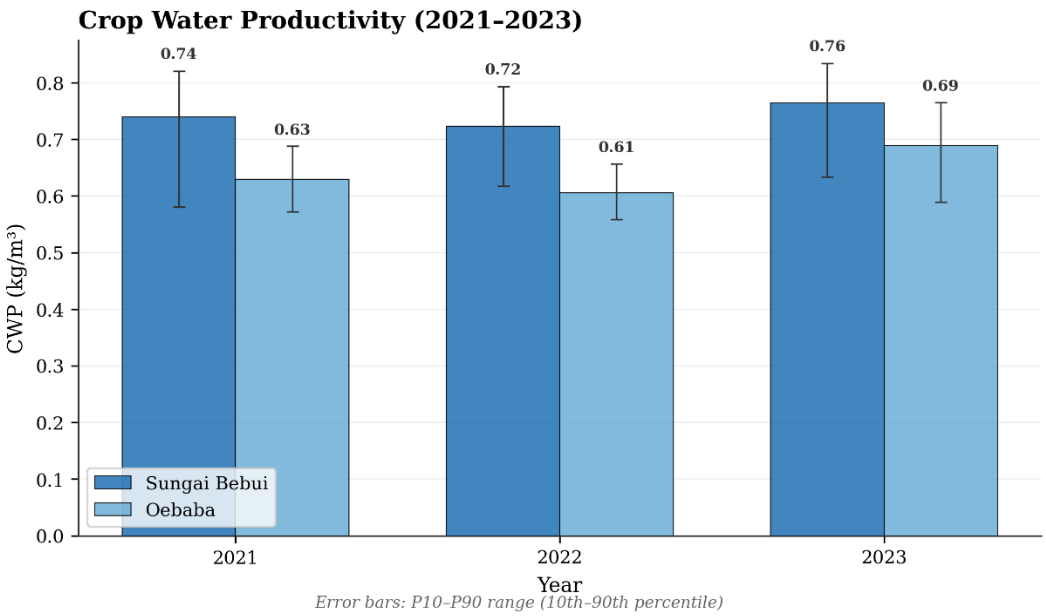

Figure 13: Rice water productivity for Sungai Bebui (left) and Oebaba (right) schemes in 2021, 2022 and 2023.

Table 3: Average, P10 and P90 rice water productivity for Sungai Bebui and Oebaba schemes in 2021, 2022 and 2023

Year	Sungai Bebui		Oebaba	
	Mean (kg/m³)	[P10–P90]	Mean (kg/m³)	[P10–P90]
2021	0.74	[0.58–0.82]	0.63	[0.57–0.69]
2022	0.72	[0.62–0.79]	0.61	[0.56–0.66]
2023	0.76	[0.63–0.83]	0.69	[0.59–0.76]

Table 4: Average yield, CWP, AETI and AGBP for rice in Sungai Bebui and Oebaba in 2021 - 2023

Year	Sungai Bebui				Oebaba			
	Yield (t/ha)	CWP (kg/m³)	AETI (mm)	AGBP (kg DM/ha)	Yield (t/ha)	CWP (kg/m³)	AETI (mm)	AGBP (kg DM/ha)
2021	2.78	0.74	367	6,952	2.90	0.63	460	7,253
2022	3.01	0.72	414	7,523	2.96	0.61	490	7,397
2023	3.17	0.76	410	7,918	3.03	0.69	440	7,587

Figure 14 shows the relation between rice yield and actual evapotranspiration for experimental fields across 17 countries (2000 - 2010), visualizing the position of the CWP computed for Oebaba and Sungai

Bebui (due to their proximity in this feature space, both are represented by a single symbol). This implies that, when considered in a global perspective, rice water productivity (as well as rice yield) in the two pilot schemes is relatively low, suggesting scope for improvement. A more recent meta-analysis of CWP values[1], disaggregating between different regions, utilizes an average rice CWP value for South East Asia of 1.01 kg/m^3 with a standard deviation of 0.45 kg/m^3, thus placing the values for Timor-Leste at the lower end of the regional range. At the global level, the study classifies "Medium" rice CWP as >0.70 to ≤1.25 kg/m^3 and "Low" as below 0.7 kg/m^3, implying that Sungai Bebui performs at the lower end of "Medium" and Oebaba at the upper end of the "Low" category.

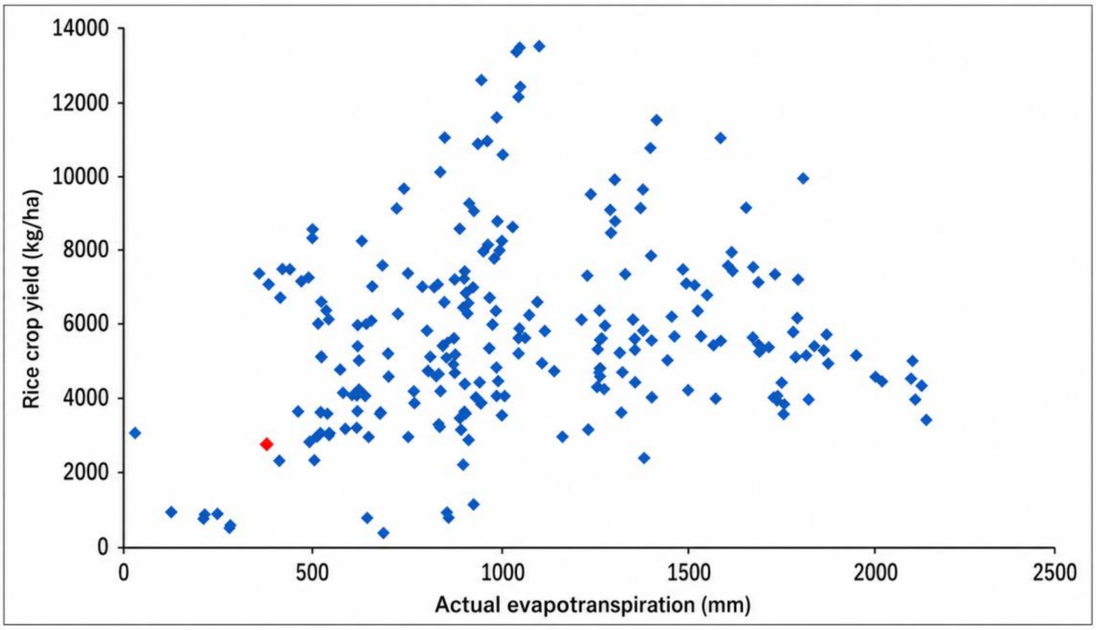

Figure 14: Rice Water Productivity in Sungai Bebui and Oebaba (in red) in relation to measurements in experimental fields during the period of 2000 to 2010 in 17 countries (adapted from Bastiaanssen et al., 2012[2]).

[1] *Foley, D. J., Thenkabail, P. S., Aneece, I. P., Teluguntla, P. G., & Oliphant, A. J. (2020). A meta-analysis of global crop water productivity of three leading world crops (wheat, corn, and rice) in the irrigated areas over three decades. International Journal of Digital Earth, 13(8), 939–975. https://doi.org/10.1080/17538947.2019.1651912*

[2] *Bastiaanssen, W.G.M., I.J. Miltenburg and R. Goudriaan, 2012a. Water Productivity Mapping: Moderate Resolution Water Productivity Modelling and Mapping of Wheat and Maize for Morocco and Syria Using ETLook, Report to Land and Water Division FAO, Rome, Italy.*

5 Conclusions and Recommendations

This study has demonstrated that remote sensing provides a practical and scalable basis for mapping rice area, estimating rice yield, and assessing crop water productivity in Timor-Leste's irrigated rice systems. By combining high-resolution Sentinel imagery with satellite-derived evapotranspiration and biomass products in Google Earth Engine, the analysis was able to generate spatially explicit information for the two pilot schemes in a context where field-based data on rice extent, production, and water use are limited. The resulting workflow offers a foundation for supporting MALFF in monitoring rice systems more consistently and objectively, while also creating a basis for future replication in other parts of the country.

A key conclusion from this work is that the methodology is suited for upscaling to other rice-producing areas in Timor-Leste. The approach relies primarily on globally available datasets and cloud-based processing, which means that it can be transferred without requiring extensive local data infrastructure. This is an important advantage in a national context where timely and spatially detailed agricultural information is often lacking. At the same time, the pilot application also shows that upscaling should not be understood as a simple copy-paste exercise. Local rice systems differ in irrigation conditions, crop calendars, topography, and management practices, and these differences need to be considered when applying the method elsewhere. For this reason, the approach is most powerful when implemented as a flexible framework that can be adapted to local conditions.

In-field observations from extension officers underline that rice systems in Timor-Leste are dynamic and can change substantially from year to year in response to hydroclimatic and pest-related pressures. Even within the same scheme, planting and harvesting may differ between fields depending on water availability, farmer decisions, and operational realities. A main strength of the developed methodology is, therefore, that it detects rice phenology from satellite observations and subsequently defines field-specific growing seasons, rather than literature-based or fixed calendar assumptions.

The developed methodology also comes with a number of limitations. The rice mapping results are considered more robust than the absolute yield and crop water productivity estimates, since rice extent can be detected more directly from high-resolution temporal patterns in satellite imagery. By contrast, the yield and water productivity calculations depend on additional assumptions, including the use of biomass and evapotranspiration products at coarser resolution and the translation of biomass into grain yield. As a result, the output is particularly valuable for identifying relative spatial patterns, interannual differences, and contrasts between fields or schemes. In the absence of field data for calibration and validation, absolute values should be interpreted with greater caution. Further improvement of the methodology would be possible through refinement of the harvest index, ideally moving towards locally calibrated values or stress-sensitive adjustments rather than one fixed parameter for all situations.

Future linking of the remote-sensing workflow to targeted field campaigns is therefore recommended. Field measurements of harvested yield, crop management, and planting dates in selected plots would provide the evidence needed to calibrate and validate the satellite-based estimates more rigorously. Such field campaigns would also help to better understand the causes of observed spatial variability and to distinguish between differences driven by water supply, agronomic practices, pest pressure, or other factors. In this sense, remote sensing and field data should not be seen as alternatives, but as complementary sources of information that are strongest when used together.

With regard to insitutional uptake of the developed methodology, an online presentation is foreseen where FutureWater experts will present the methodology and results, explain strengths and limitations of the applied data and methods as well as any assumptions made, and be available for answering any questions from MALFF GIS experts and other government agencies. In addition, all scripts developed under this study, as well as a video with stepwise instructions, will be shared with FAO and MALFF.

Looking ahead, further training is likely necessary to move from demonstration to sustained operational use. While the current project provides an important starting point, routine application by national staff will require familiarity not only with the technical workflow in Google Earth Engine, but also with interpretation of results, awareness of uncertainties, and integration of remote-sensing outputs into agricultural decision-making. Follow-up support could therefore focus on hands-on application to additional schemes, interpretation of results against field realities, and gradual refinement of the methodology as more local data become available.

Annex: Seasonal AETI and AGBP maps

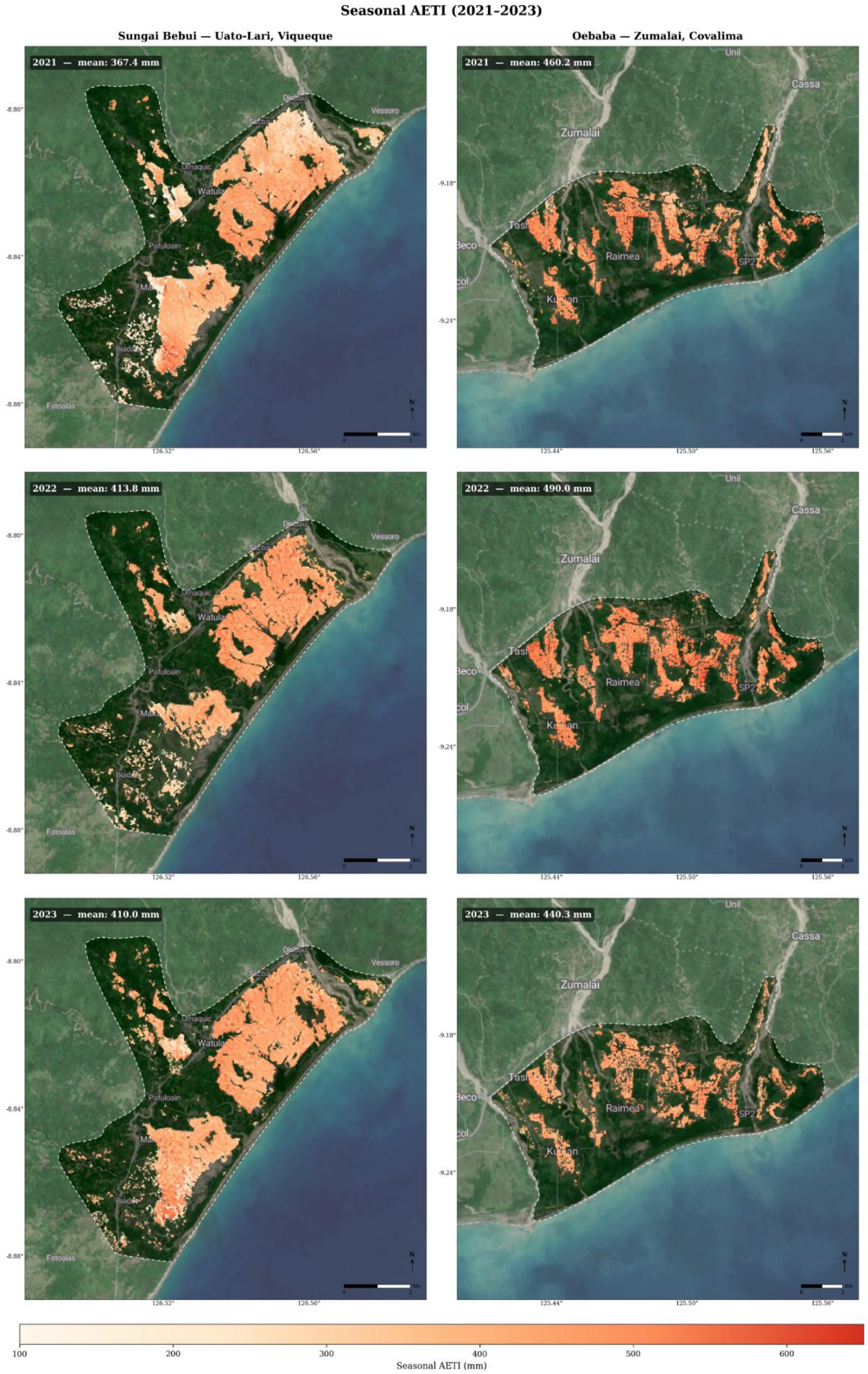

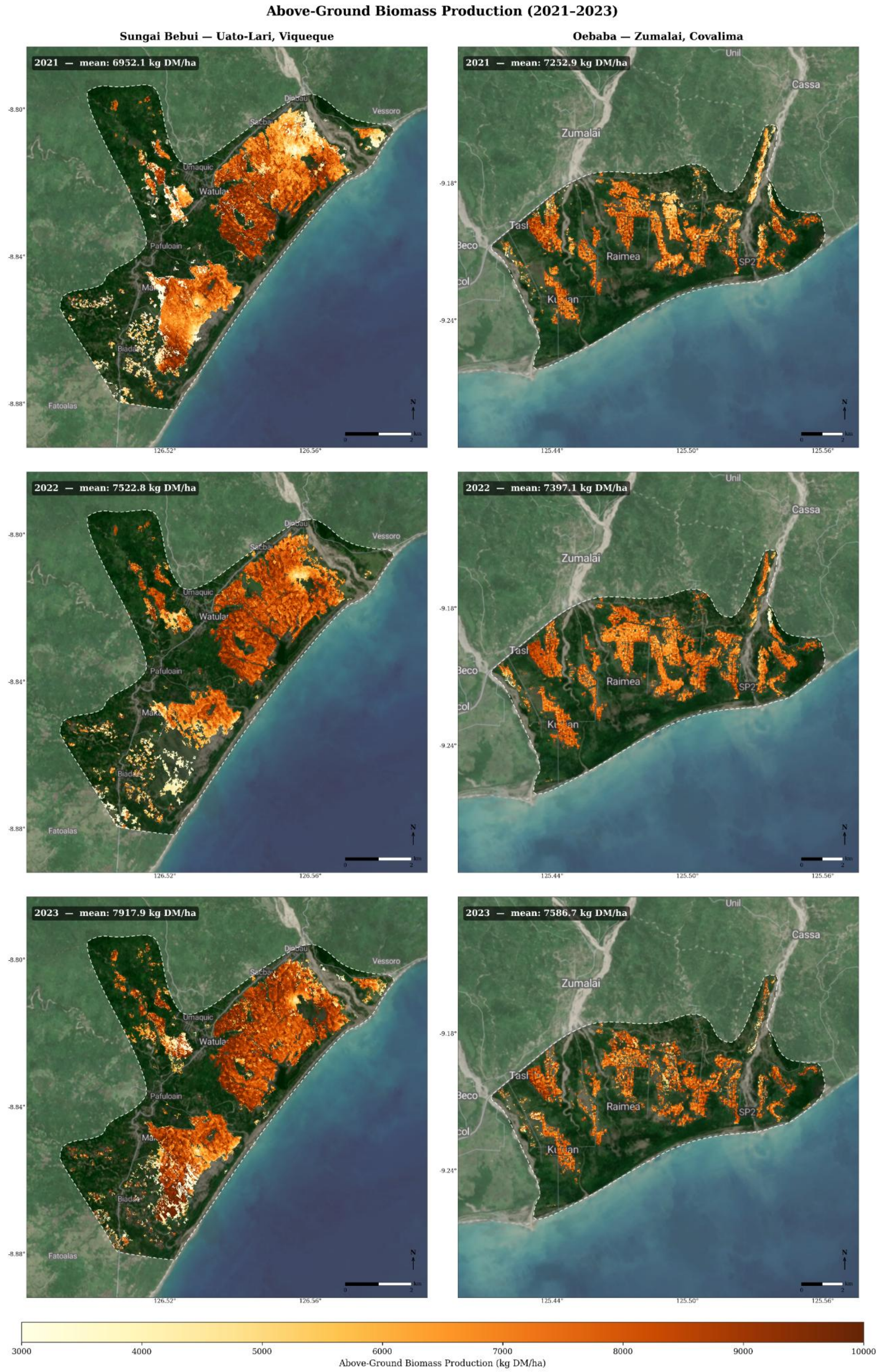
Above-Ground Biomass Production (2021-2023)
Sungai Bebui — Uato-Lari, Viqueque
Oebaba — Zumalai, Covalima
2021 — mean: 6952.1 kg DM/ha
2021 — mean: 7252.9 kg DM/ha
2022 — mean: 7522.8 kg DM/ha
2022 — mean: 7397.1 kg DM/ha
2023 — mean: 7917.9 kg DM/ha
2023 — mean: 7586.7 kg DM/ha
3000
4000
5000
6000
7000
8000
9000
10000
Above-Ground Biomass Production (kg DM/ha)